2019

A High Torque Density Halbach Rotor Coaxial Magnetic Gear

Ho Yin Wong
Portland State University, h28@pdx.edu

Jonathan Z. Bird
Portland State University, bird@pdx.edu

David Barnett
University of North Carolina at Charlotte

Wesley Williams
University of North Carolina at Charlotte

A High Torque Density Halbach Rotor Coaxial Magnetic Gear

Ho Yin (David) Wong
Department of Electrical and Computer Engineering
Portland State University
Portland, OR, USA
h28@pdx.edu

Jonathan Z. Bird
Department of Electrical and Computer Engineering
Portland State University
Portland, OR, USA
jonathan.bird@ieee.org

David Barnett
Department of Engineering Technology
University of North Carolina at Charlotte
Charlotte, NC, USA
dbarne39@uncc.edu

Wesley Williams
Department of Engineering Technology
University of North Carolina at Charlotte
Charlotte, NC, USA
wbwillia@uncc.edu

***Abstract*— This paper presents the design, analysis, and experimental testing results for a 5.67:1 Halbach rotor magnetic gearbox with a ferromagnetic back support. Using 3-D finite element analysis software the Halbach magnetic gearbox was calculated to achieve a volumetric torque density of 284N·m/L with only an active region outer diameter of 120mm. The experimental prototype obtained an active region volumetric torque density of 261.4N·m/L**

Keywords— Magnetic gear, permanent magnet, Halbach array

I. INTRODUCTION

MECHANICAL gearboxes require routine servicing and lubrication due to wear from contacting gear teeth. Some gearing systems are not back-drivable and most offer limited compliance capabilities, a mechanical gearing system can also have a large starting torque [1], [2]. A MG utilizes magnetic field space modulation to achieve speed-amplification without any physical contact. If properly designed, a magnetic gearbox (MG) has the potential to eliminate most of the problems associated with mechanical gears and in addition offers the capability of increasing power conversion efficiency and inherent overload protection [3].

One of the main obstacles to the wide-spread use of MGs is that the torque density of the currently developed MGs is still not high enough to be competitive with their mechanical gearbox counterparts. For instance, mechanical gearboxes with torque densities well in excess of 300 N·m/L are achievable [2], [4], yet the development of MGs to-date still struggle to breakthrough this limit.

The object of this paper is to try to increase the torque density capability of coaxial MGs by utilizing a Halbach rotor coaxial MG. An example of a Halbach rotor flux-modulating coaxial MG is shown in Fig. 1, it consists of an inner rotor, with p_1 permanent magnet (PM) pole-pair rotating at ω_1, a middle cage rotor with n_2 ferromagnetic segments that can rotate at ω_2 and a fixed p_3 pole-pair PM outer rotor ($\omega_3 = 0$). The inner and outer rotors that contain PMs interact with the cage rotor ferromagnetic steel segments to create space harmonics. If the relationship between the steel segments is chosen to be $p_1 = n_2 - p_3$ then the rotors will interact via a common space harmonic and the angular speeds between the inner and cage rotor is [5]

$$\omega_1 p_1 = \omega_2 n_2 \tag{1}$$

In 2004 Atallah *et al.* calculated that a torque density of up to 100N·m/L is achievable when using the surface mounted PM coaxial MG [5]. More recently a flux-focusing coaxial MG typology was presented by Uppalapati *et al.* that achieved an experimentally tested torque density of 239N·m/L [6]. However, using a flux-focusing typology results in a relatively large 3rd and 5th order field harmonic being created, consequently this generates a significant amount of loss within the MG structure thereby degrading performance [7]. Halbach rotor structures are well-known for creating highly sinusoidal field distributions [8] and therefore offer the potential for both increasing torque density and lowering harmonic related losses. In 2009, Jian *et al.* studied the torque density and torque ripple performance of a 1:4.25 gear ratio Halbach rotor MG [9]. Jian's design achieved a peak torque and torque density of 155.8 N·m and 108 N·m/L respectively. In 2016, Jing *et al.* also constructed a 1:4.25 gear ratio Halbach rotor MG Jing's prototype achieved a peak torque and volumetric torque density of 168 N·m and 129.8N·m/L respectively [10].

Jian *et al.* [11] and Jing *et al.* [12] used 2-D analytic and 2-D finite element analysis (FEA) modeling technique to study the

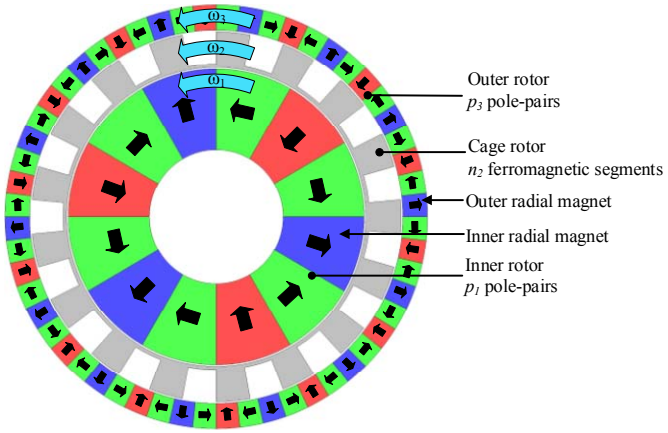

Fig. 1. A 5.67:1 coaxial Halbach rotor magnetic gearbox with p_1=3 pole-pairs, n_2=17 ferromagnetic slots and p_3=14 pole-pairs on the outer rotor.

performance of the Halbach PM rotor relative to the radial rotor MG equivalent and Gardner *et al.* developed a 2-D magnetic equivalent circuit model of the Halbach MG [13]. Jian convincingly demonstrated that the Halbach array MG could perform significantly better than the conventional radially magnetized rotor MG in terms of volumetric torque density as well as torque ripple and iron loss [11]. It should be noted that the 3-D axial edge-effects are particularly high within a MG and therefore if the axial length is less than the radius the torque will be significantly lower than what the 2-D models predict. Therefore before building a MG, extensive 3-D FEA analysis is also recommended [5], [14], [15].

As the Halbach rotor field is focused only one side the Halbach MG has the potential for being built with minimal steel. Asnani *et al.* [16] and Scheidler *et al.* [17] have recently studied the performance of MGs when using 3-D printed plastic housings. Scheidler demonstrated a MG with a volumetric torque density of 162 N·m/L and because of the all plastic housing design the mass torque density was an impressive 44.7 N·m/kg.

An axial equivalent of the Halbach rotor MG typology was also studied by Johnson *et al.* [18] with a 1:4.41 gear ratio Johnson calculated that the axial MG could operate with a volumetric torque density of 183.9 N·m/L. The axial MG can be designed with a short axial length but maintaining the uniform airgap would be challenging.

The contribution made by this paper is to use a parameter sweeping analysis to both study and experimentally test a Halbach rotor MG with the goal of demonstrating that the Halbach typology enables torque densities close to 300 N·m/L to be within reach.

II. 2-D Magnetic Design Analysis

The investigation procedure for the Halbach rotor MG typology began with the ideal Halbach rotor MG structure as shown in Fig. 1. A simple cage modulator design with a 1mm thick inner bridge was used. Table I shows the fixed geometric MG parameters that were not changed in the design analysis and Table II shows the radial sweep parameter values. The parameters are defined in Fig. 2. Based on prior experience the three rotor's radial lengths, along with axial length, d, have the biggest impact on the torque density.

The torque ripple of the MG remains essentially unchanged with respect to the load, hence, cogging torque and torque ripple within the MG are the same [19]. The torque ripple can be minimized by selecting a pole combination in which the greatest common divisor (gcd) defined as [20], [21].

$$C_T = \gcd(2p_1, n_2) \tag{2}$$

is minimized. For this Halbach rotor design the pole combination (p_1, n_2, p_3) = (3,17,14) was selected, this gives a gear ratio of G_{12}=5.67 and using (2) gives C_T= 1. Therefore, it is expected the torque ripple will be low. It should however be noted that because the cage rotor is an odd number the radial forces on the cage rotor are unsymmetrical [20].

In the following analysis the magnets are Nd-Fe-B, grade N48, and the laminations are M19 steel. The outer radius and axial length of the MG have been fixed at r_{o3} = 60mm and d=50mm respectively. The radial parameters, identified in Table 2 were swept across the defined range of values and the resultant 2-D FEA calculated torque density for each parameter value is shown in Fig. 3.

The active region volumetric torque density was computed from

$$T_v = T_2/(\pi r_{o3}^2 d) \tag{3}$$

where T_2 = cage rotor torque. And the active region mass torque density was computed using

$$T_m = T_2/(m_s + m_m) \tag{4}$$

where m_s and m_m are the ferromagnetic steel and magnet material mass respectively.

Looking at the zoomed in view in Fig. 3(b) it can be seen that a clear trade-off between maximizing mass torque density, *Design A*, and volumetric torque density, *Design B*, is present. Note that since the outer radius was fixed at r_{o3} = 60mm when the modulation length, l_2, was changed, the outer rotor inner radius r_{i3} was also changed since $r_{i3} = r_{o1}+l_2+2g$.

TABLE I. Halbach Magnetic Gearbox Fixed Geometric Parameters

Description		Value	Unit
Inner rotor	Pole pairs, p_1	3	-
	Angular span, θ_1	$\pi/(2p_1)$	radians
Cage rotor	Pole pairs, n_2	17	-
	Angular span, θ_2	$\pi/(n_2)$	radians
Outer rotor	Outer radius, r_{o3}	60	mm
	Pole pairs, p_3	14	-
	Angular span, θ_3	$\pi/(2p_3)$	radians
Axial stack length, d		50	mm
Air gaps, g		0.5	mm

TABLE II. Sweep Parameters

Description	Sweep values [mm]
Inner radius, r_{i1}	[8, 10, … 30]
Inner rotor outer radius, r_{o1}	[30, 32, … 50]
Cage bar length, l_2	[2.5, 3, … 7.5] & [8, 9, … 13]

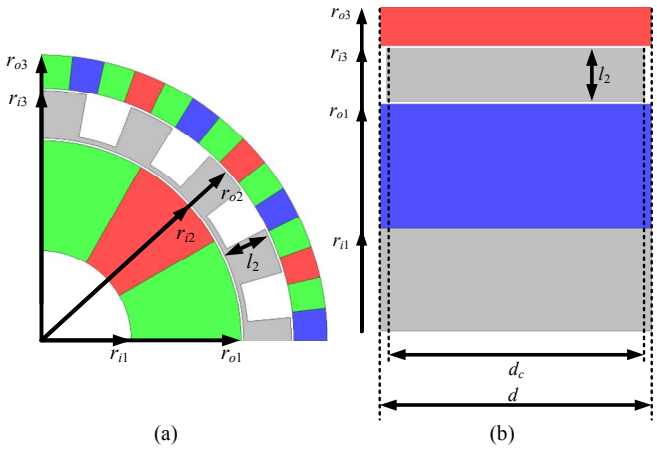

(a) (b)

Fig. 2. Geometric parameter definitions along (a) radial and (b) axial lengths.

The design parameters for the peak mass and volumetric torque density design are shown in Table III. Also shown is a trade-off design, *Design C*, in which both a relatively high mass and volumetric torque density is obtained whilst the parameters are relatively mechanically strong and feasible to construct. The geometry for this *Design C* was used to create Fig. 1.

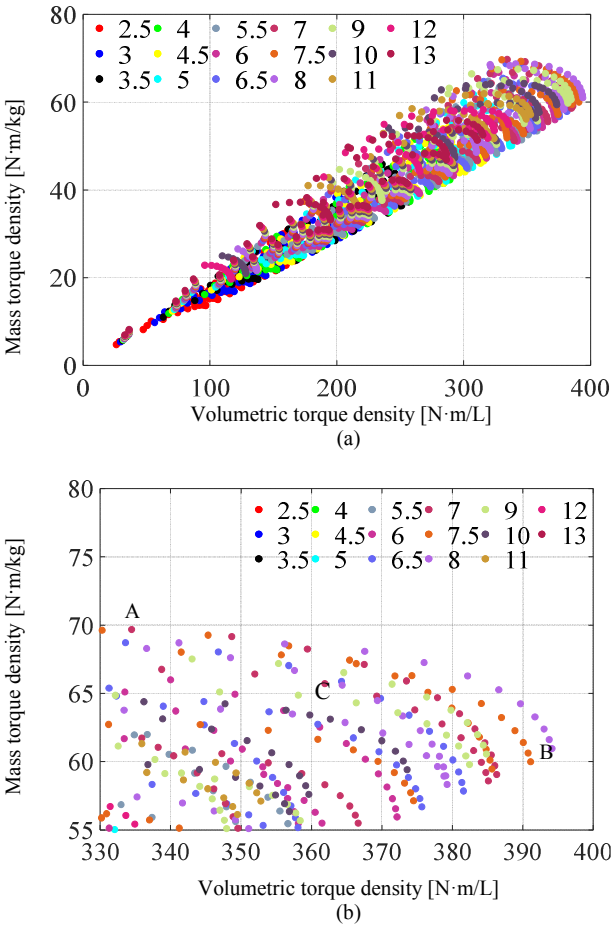

Fig. 3. (a) Volumetric and mass torque density trade-off plot and (b) zoomed in view. The legend shows the different cage rotor length, l_2, values. *Design A* has the highest mass torque density and *Design B* has the highest volumetric torque density and *Design C* is the trade-off design shown in Fig. 1.

TABLE III DESIGN CHOICES

Parameter	Maximum torque density		Trade-off design (C)	Unit
	Mass (A)	Volume (B)		
Inner rotor inner radius, r_{i1}	30	8	19	mm
Inner rotor outer radius, r_{o1}	46	44	42	mm
Modulator radial length, l_2	7	8	10	mm
Inner radius of outer rotor	54	53	53	mm
Peak torque	189.2	222.9	203.5	N·m
Volumetric torque density	334.6	394.2	359.9	N·m/L
Mass torque density	69.7	60.9	63.4	N·m/kg
Magnet mass torque density	84.5	71	78.7	N·m/kg

III. MECHANICAL CONSIDERATIONS

The *Design C* cage rotor lamination was modified in order to provide mechanical support. Rectangular slots and lips were added to the cage rotor, as shown in Fig. 4, this provided the necessary retaining support to allow rectangular Garolite, G10, rods to be used to support the cage rotor in place. The Garolite material was selected because it provided the radial deflection support for the cage rotor and this therefore reduced the power losses by eliminated all non-laminated conductive parts from the cage rotor. For ease of assembly, ferromagnetic back support material was added to the outer and inner radius as shown in Fig. 4. Due to mechanical design requirements the inner rotor shaft, and the inner rotor back support is a solid cylinder with radius of r_{i1}. However, the outer rotor ferromagnetic back support thickness, l_b, remains adjustable. Fig. 5 shows how the torque performance with different outer rotor back support thicknesses affect the torque and torque density. As the back-support steel thickness increases, the torque decreases until it reaches a plateau. The use of the ferromagnetic back-support provides mechanical fabrication support and greatly helps with magnet assembly. A back-support thickness l_b = 3mm was selected. After making these mechanical design changes the resultant 2-D FEA calculated peak torque reduced to 193.5 N·m and consequently the volumetric and mass torque density reduced to 342.2 N·m/L and 52.2 N·m/kg respectively.

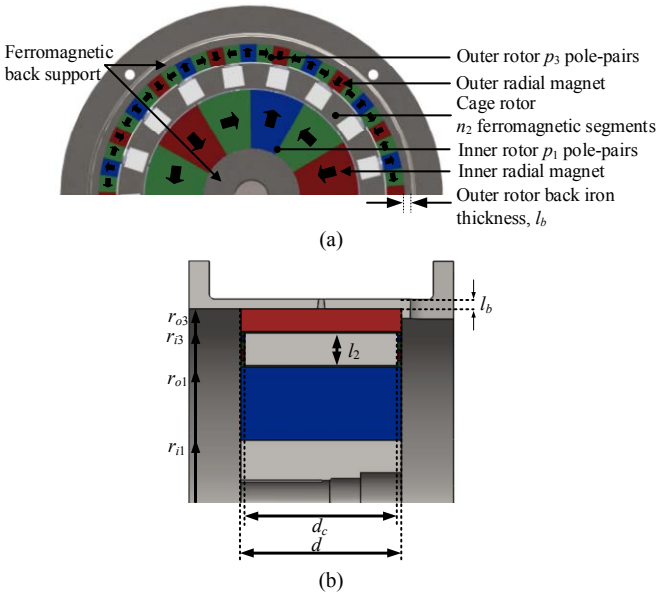

Fig. 4. (a) Half cut-away view of the Halbach rotor magnetic gearbox and (b) axial view of the magnetic gearbox .

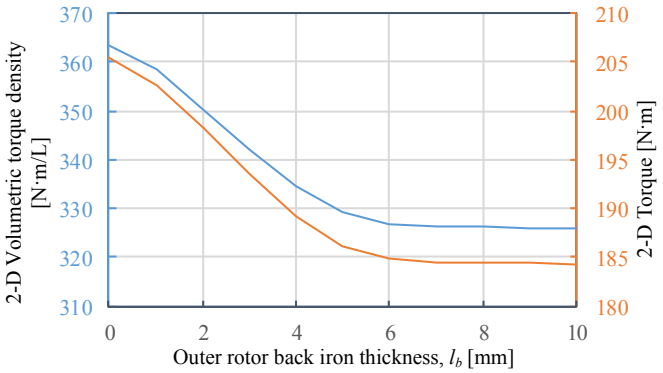

Fig. 5. Influence of torque and torque density when the outer rotor ferromagnetic back-support thickness, l_b, is increased.

IV. 3-D Magnetic Analysis

The impact of the axial length, d, on the Halbach MG performance is shown in Fig. 6. An axial length of d = 50mm was selected as this still maintained a high torque and volumetric torque density whilst the radial deflection forces were determined to be not serious at this axial length.

Gerber *et al.* showed that if the modulator rotor axial length was reduced slightly the torque density could be improved [22]. Fig. 7 demonstrates the torque performance at different cage lamination axial lengths, d_c, when the inner and outer rotor axial lengths were kept fixed at d = 50mm. It can be seen that a peak torque density occurs when d_c = 47.5mm, this therefore increased the torque and torque density to 160.6 N·m and 284 N·m/L, a 1.3% improvement. This d_c value was selected for the cage axial length.

The 3-D FEA calculated torque versus cage rotor angle over one pole-pair span and the torque ripple for the final design at peak torque angle are shown in Fig. 8. The calculated torque ripple is low with a calculated value of 0.58 % at peak torque.

A contour plot showing the magnitude of the flux density, $\mathbf{B}_r$, $\mathbf{B}_\theta$ and $|\mathbf{B}|$, within the MG is shown in Fig. 9. The saturation along the bridges is apparent.

The operating principle of the MG can be verified by considering the analysis shown in Fig 10 in which the harmonics created next to the outer rotor airgap for the case when *only* the inner rotor is present and when both the inner rotor and cage rotor are present. It can be seen that the inclusion of the cage rotor creates the necessary p_3 = 14 spatial harmonic.

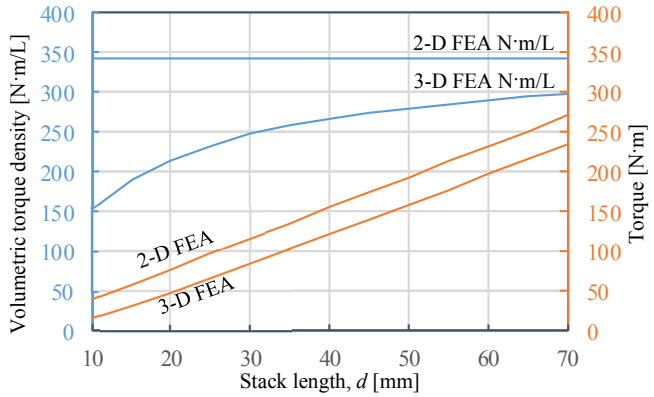

Fig. 6. Impact of stack length on the peak torque and volumetric torque density when axial length of MG is increased.

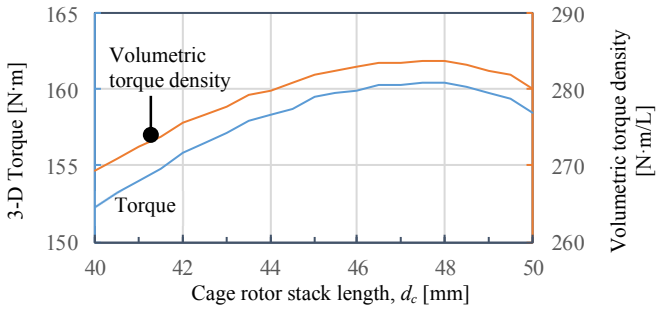

Fig. 7. Impact of cage rotor lamination stack length on the peak torque when inner and outer rotor stack length is d = 50 mm.

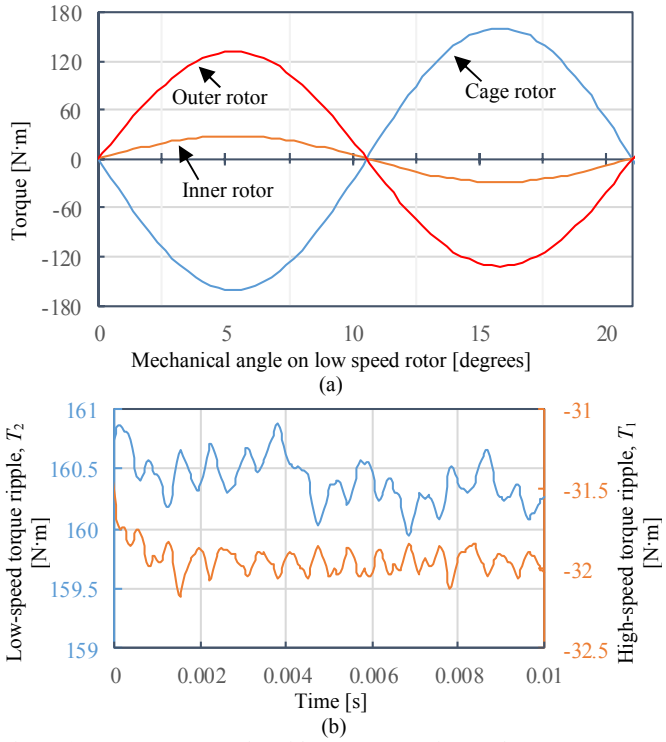

Fig. 8. (a) 3-D FEA torque plot with two rotors stationary (b) 3-D FEA torque ripple plot with cage rotor rotating at 180RPM and inner rotor rotating at 1020RPM according to gear ratio at peak torque angle.

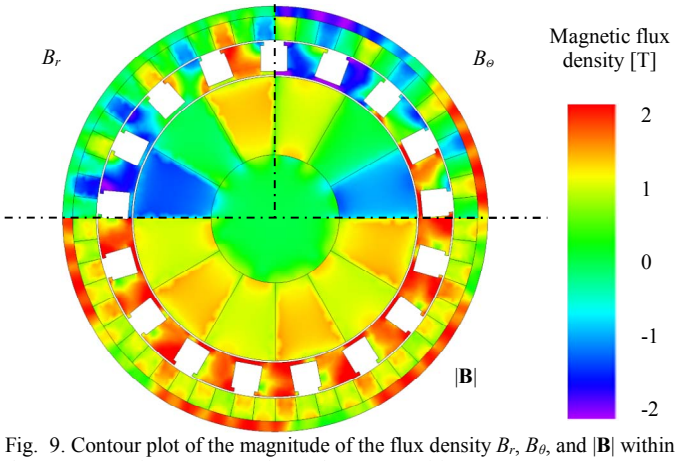

Fig. 9. Contour plot of the magnitude of the flux density B_r, B_θ, and $|\mathbf{B}|$ within the MG magnetic structure at the peak torque position.

V. Experimental Prototype

The assembled individual MG rotors are shown in Fig. 11. In the prototype, both the inner and outer rotor back supports were made with solid steel instead of laminations due to the limited time. In addition, to reduce eddy current loss due to axial edge effects and axial flux leakage, non-magnetic, non-conductive, material was used on the axial cage and outer rotors end plate. Magnets are attached to the rotors' back supports with glue.

The radial magnetic flux density created by the assembled inner and outer rotors were measured manually at an air-gap of 0.63mm, the measurement results are compared in Fig. 12 and

Fig. 13 with the 2-D and 3-D FEA calculated values. A relatively good match was achieved.

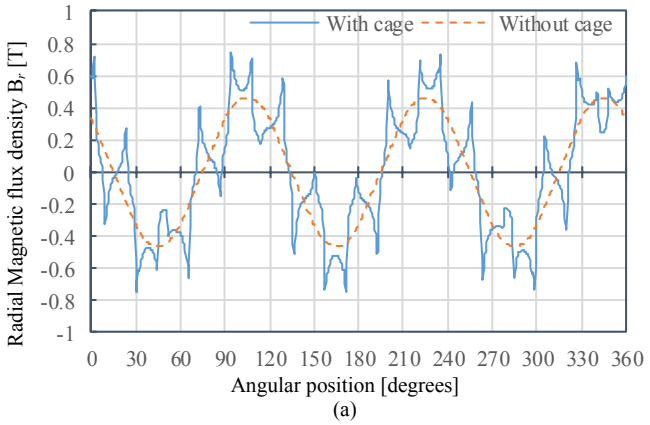

(a)

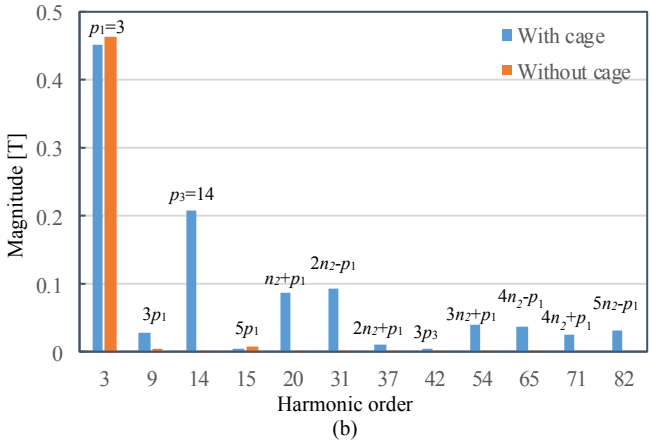

(b)

Fig. 10. 3-D FEA radial magnetic flux density field plot next to the outer rotor for the case when only the inner rotor is present and also when both the inner rotor and cage rotor is present, but not the outer rotor. (b) The corresponding spatial harmonics spectrum. It can be seen that when the cage rotor is added, the $p_3 = n_2 - p_1$ harmonic is created.

(a)

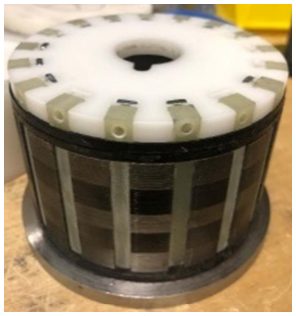

(b)

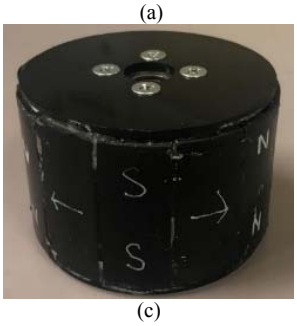

(c)

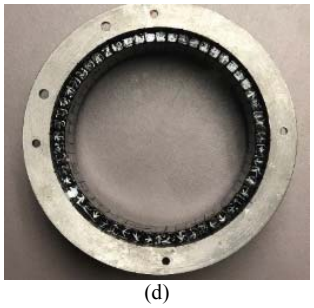

(d)

Fig. 11.(a) Cage rotor lamination. (b) Assembled cage rotor with Garolite supporting bars. (c) Assembled inner rotor with Halbach array magnet embedded. (d) Assembled outer rotor with Halbach array magnet embedded.

Fig. 12 and Fig. 13 harmonic analysis show that the inner rotor magnet field is 7.9 % higher than the 3-D FEA model predicted whereas the outer rotor magnets field is 10.7 % lower than the 3-D FEA model predicted.

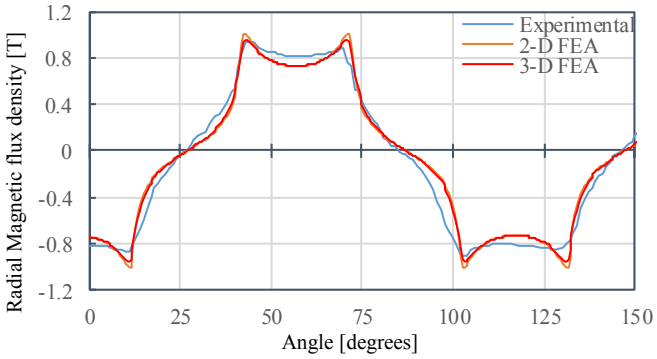

(a)

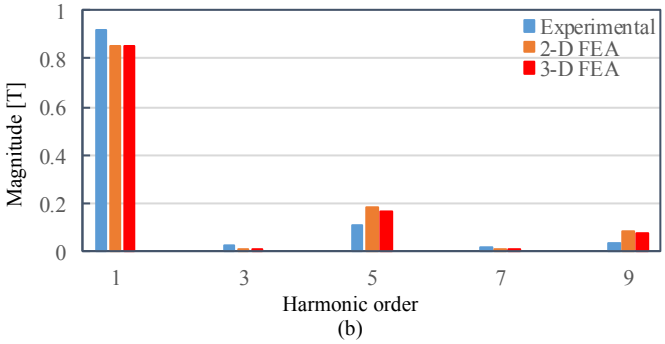

(b)

Fig. 12.(a) Inner rotor radial flux density field comparison over one pole and (b) corresponding harmonic analysis comparison when measured and calculated with an airgap of 0.63mm (half the Gaussmeter probe thickness).

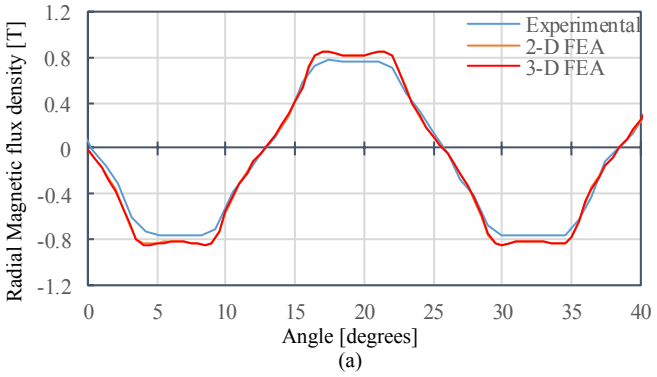

(a)

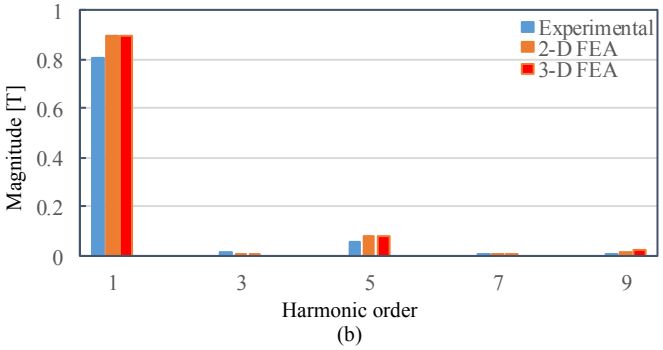

(b)

Fig. 13.(a) Outer rotor radial flux density field comparison over one pole and (b) corresponding harmonic analysis comparison when measured and calculated with an airgap of 0.63mm (half the Gaussmeter probe).

The fully assembled MG is shown in Fig. 14(a) and also shown in Fig. 14 (b) is a mechanical cut-away view of the assembly. Fig. 15 shows the MG on the test setup. The torque transducers on either side of the MG are being used to characterize the torque-speed and efficiency characteristics.

VI. Experimental Testing Results

The torque as a function of load angle was measured by locking the inner rotor and rotating the cage rotor. The resulting torque measurements are shown in Fig. 16. It can be seen that a peak torque of 147.8 N·m was achieved, this is 8 % lower than was computed using 3-D FEA. Table IV. summarizes the performance results.

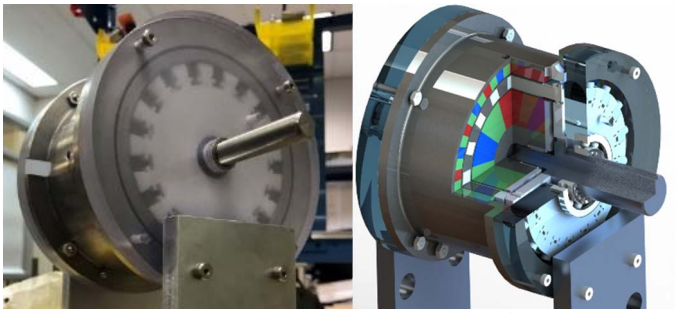

(a) (b)

Fig. 14. (a) Fully assembled prototype photo (b) Section view of the built prototype CAD image.

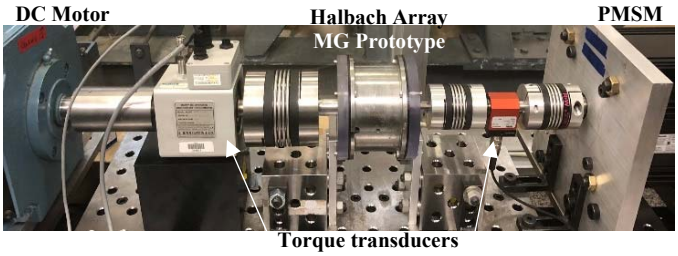

Fig. 15. Experimental torque measurement setup.

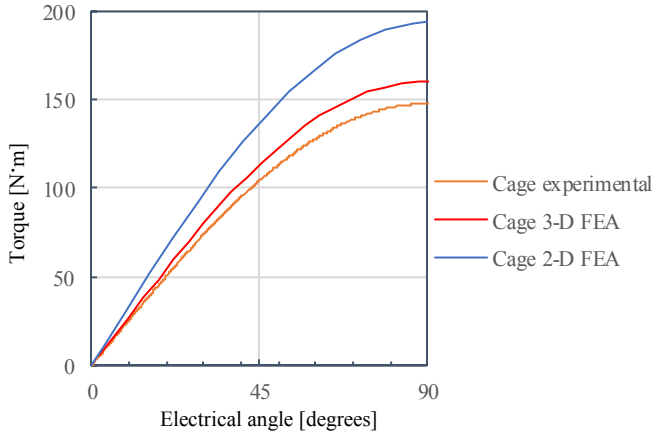

Fig. 16 . 2-D FEA vs 3-D FEA vs Experimental cage rotor pole-slip plot over 90 degrees electrical angle.

A plot of the measured torque as a function of time is shown in Fig. 17. The permanent magnet synchronous motor (PMSM) was set to speed control mode and the DC motor was in torque control mode to imitate the load. The operation at constant torque for two cases at 55 N·m and then at 105 N·m is shown.

The torque ripple was significantly higher than expected at 16.3N·m, 11% at peak torque, the reason for this is currently being investigated and maybe a result of unwanted mechanical vibrations in the setup or an eccentric air gap. Fig. 18 shows the no load torque measurement for both rotors.

Table IV Final Prototype Parameter

Description		Prototype	Calculated	Unit
Active region torque density	Peak torque	147.8	160.6	N·m
	Volumetric	261.4	284	N·m/L
	Mass	39.9	43.4	N·m/kg
	Magnet mass	57.2	62.1	N·m/kg
Full assembly Dimension	Outer diameter	150	-	mm
	Axial length	114.3	-	mm
	Mass	6.6	-	kg
Full assembly torque density	Volumetric	73.2	-	N·m/L
	Mass	22.4	-	N·m/kg

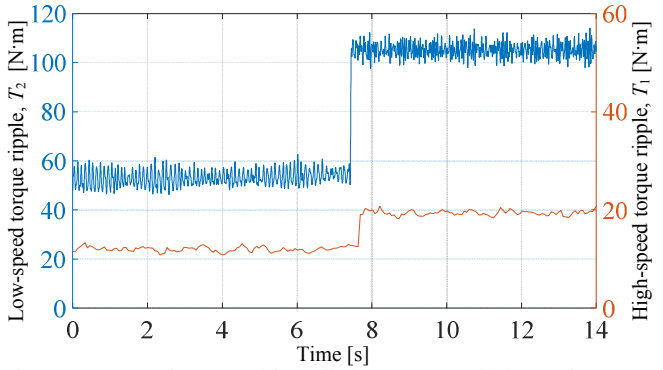

Fig. 17. Measured torque with applied 300RPM on high speed rotor and changing load on low speed rotor.

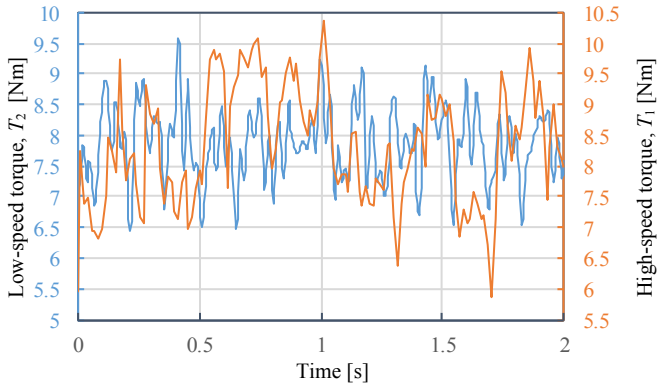

Fig. 18 Measured no load torque for both low speed and high speed rotor at 50 RPM and 225RPM respectively.

VII. Conclusion

This paper has presented the design, analysis and initial experimental testing results for a high torque density coaxial MG with Halbach rotors. The calculated 3-D FEA peak torque and volumetric torque density was 160.6 N·m and 284 N·m/L whilst the measured peak torque was 147.8 Nm and this corresponds to an active region torque density of 261.4 N·m/L.

The measured torque ripple was unfortunately higher than expected and the reason for this is currently being investigated.

Future designs will be changed to using an even number of cage rotors bars so as to minimize unsymmetrical radial forces that can cause increased bearing wear.

Acknowledgments

This work was supported by the National Science Foundation under award 1636704 and award number 1827801. Additional funding support was provided through the North Carolina Coastal Studies Institute's ocean energy research program. The authors would like to thank the JMAG Corporations for the use of their FEA software.

References

[1] J. W. Titus, "Analysis of Friction Torque in Simple and Preloaded Spur Gear Trains." Naval Research Lab Washington DC, 1965.

[2] "Nabtesco Cycloidal Gearbox." . Available: http://www.nabtescomotion-control.com/products/.

[3] P. O. Rasmussen, T. O. Andersen, F. T. Joergensen, and O. Nielsen, "Development of a high performance magnetic gear," in *38th IAS Annual Meeting on Conference Record of the Industry Applications Conference, 2003.*, 2003, vol. 3, pp. 1696–1702 vol.3.

[4] "Sm-Cyclo Speed Reducers and Gearmotorsed: Series 4000." Sumitomo Machinary Corporation of America.

[5] K. Atallah, S. D. Calverley, and D. Howe, "Design, analysis and realisation of a high-performance magnetic gear," *IEE Proc. - Electr. Power Appl.*, vol. 151, no. 2, pp. 135–143, Mar. 2004.

[6] K. K. Uppalapati, J. Z. Bird, J. Wright, J. Pitchard, M. Calvin, and W. Williams, "A magnetic gearbox with an active region torque density of 239Nm/L," in *2014 IEEE Energy Conversion Congress and Exposition (ECCE)*, 2014, pp. 1422–1428.

[7] K. Li, S. Modaresahmadi, W. Williams, J. Wright, J. Bird, and D. Som, "Designing and Experimentally Testing a Magnetic Gearbox for a Wind Turbine Demonstrator," *IEEE Trans. Ind. Appl.*, pp. 1–1, 2019.

[8] K. Halbach, "Design of permanent multipole magnets with oriented rare earth cobalt material," *Nucl Instr Meth*, vol. 187, pp. 1–10, 1980.

[9] L. Jian, K. T. Chau, Y. Gong, J. Z. Jiang, C. Yu, and W. Li, "Comparison of Coaxial Magnetic Gears With Different Topologies," *IEEE Trans. Magn.*, vol. 45, no. 10, pp. 4526–4529, Oct. 2009.

[10] L. B. Jing, Y. J. Zhang, C. Li, and H. Zhang, "Magnetic Analysis and Design Optimization of Halbach Array Coaxial Magnetic Gearbox," *PCSEE*, vol. 33, no. 21, pp. 163–169, 2013. (In Chinese)

[11] L. Jian and K. T. Chau, "A Coaxial Magnetic Gear With Halbach Permanent-Magnet Arrays," *IEEE Trans. Energy Convers.*, vol. 25, no. 2, pp. 319–328, Jun. 2010.

[12] L. B. Jing and Y. J. Zhang, "Exact analytical method for magnetic field computation in the concentric magnetic gear with Halbach permanent-magnet arrays," in *2013 IEEE International Conference on Applied Superconductivity and Electromagnetic Devices*, 2013, pp. 343–346.

[13] M. C. Gardner, D. A. Janak, and H. A. Toliyat, "A Parameterized Linear Magnetic Equivalent Circuit for Air Core Radial Flux Coaxial Magnetic Gears with Halbach Arrays," in *2018 IEEE Energy Conversion Congress and Exposition (ECCE)*, 2018, pp. 2351–2358.

[14] S. Gerber and R. Wang, "Evaluation of a prototype magnetic gear," in *2013 IEEE International Conference on Industrial Technology (ICIT)*, 2013, pp. 319–324.

[15] M. C. Gardner, B. E. Jack, M. Johnson, and H. A. Toliyat, "Comparison of Surface Mounted Permanent Magnet Coaxial Radial Flux Magnetic Gears Independently Optimized for Volume, Cost, and Mass," *IEEE Trans. Ind. Appl.*, vol. 54, no. 3, pp. 2237–2245, Jun. 2018.

[16] V. Asnani, J. Scheidler, and T. Tallerico, "Magnetic gearing research at NASA." AHS International 74th Annual Forum & Technology Display, Phoenix, Arizona, 14-May-2018.

[17] J. J. Scheidler, V. M. Asnani, and T. F. Tallerico, "NASA's Magnetic Gearing Research for Electrified Aircraft Propulsion," in *2018 AIAA/IEEE Electric Aircraft Technologies Symposium (EATS)*, 2018, pp. 1–12.

[18] M. Johnson, M. C. Gardner, and H. A. Toliyat, "Analysis of axial field magnetic gears with Halbach arrays," in *2015 IEEE International Electric Machines & Drives Conference (IEMDC)*, 2015, pp. 108–114.

[19] N. Niguchi and K. Hirata, "Cogging Torque Analysis of Magnetic Gear," *IEEE Trans. Ind. Electron.*, vol. 59, no. 5, pp. 2189–2197, May 2012.

[20] G. Jungmayr, J. Loeffler, B. Winter, F. Jeske, and W. Amrhein, "Magnetic gear: Radial force, cogging torque, skewing and optimization," in *2015 IEEE Energy Conversion Congress and Exposition (ECCE)*, 2015, pp. 898–905.

[21] Z. Q. Zhu and D. Howe, "Influence of design parameters on cogging torque in permanent magnet machines," in *1997 IEEE International Electric Machines and Drives Conference Record*, 1997, p. MA1/3.1-MA1/3.3.

[22] S. Gerber and R. Wang, "Analysis of the end-effects in magnetic gears and magnetically geared machines," in *2014 International Conference on Electrical Machines (ICEM)*, 2014, pp. 396–402.